20-GHz-to-1-THz Repetition Rate Pulse Sources Based on Multiple Four-Wave Mixing in Optical Fibers

Julien Fatome, Stéphane Pitois, and Guy Millot

***Abstract*—In this paper, we theoretically and experimentally study the generation of very high-repetition-rate pulse sources based on multiple four-wave mixing in optical fibers. More precisely, we described the generation of nearly transform-limited pulses at repetition rates of 20, 40, 80, 160, 320, 640 GHz, and 1 THz with a wavelength tunability close to 20 nm around 1555 nm. In particular, frequency resolved optical gating analyses show that 170-fs transform-limited pulses have been generated at 1 THz.**

***Index Terms*—Nonlinear optics, optical fiber, pulse generation, ultrafast optics.**

I. Introduction

LASER sources emitting pico- and femtosecond pulses at very high repetition rates are now widely employed in several domains of physics and their development constitutes a very active research area. For example, in future optical networks, the use of high bit rates per channel is a promising way towards the reduction of cost per bit. The feasibility of such ultra-high-capacity optical communication systems has been proved by many transmission experiments reported in the literature [1], [2]. One of the most remarkable results is the transmission of 1.28 and 2.56 Tbit/s over more than 160 km of optical fiber [1]. Clock generation [3], optical waveform measurement based on optical-sampling [4] and generation of millimeter-wave signals [5] are also important applications of very high-repetition-rate sources. Finally, such lasers can be used for testing photonic components and constitute for example an efficient tool to characterize optical regenerator devices such as nonlinear optical loop mirrors [6], [7] or saturable absorbers [8].

The most common technique for generating high-repetition-rate sources is based on the external amplitude modulation of a continuous laser source. This simple and stable method is widely used in telecommunication systems since it allows the generation of coded pulse trains. Although such method, limited by the bandwidth of the electronic system used, is not suitable for generating pulse trains at repetition rates higher than 100 GHz, it can be combined with the optical temporal multiplexing technique to obtain very high-repetition-rate pulse trains [1], [2]. The main drawback of this technique is that it requires a complex and expensive setup.

Manuscript received January 23, 2006; revised June 30, 2006.

The authors are with the Laboratoire de Physique de l'Université de Bourgogne, Centre National de la Recherche Scientifique (CNRS), UMR 5027, 21078 Dijon, France (e-mail: jfatome@u-bourgogne.fr; spitois@u-bourgogne.fr; Guy.Millot@u-bourgogne.fr).

Digital Object Identifier 10.1109/JQE.2006.881826

To overcome the limit of electronic bandwidth, all-optical nonlinear techniques were proposed. In 1984, modulational instability of a pump wave induced by a small signal was first suggested by Hasegawa [9] and experimentally realized in 1986 by Tai *et al.* [10]. Another nonlinear method is based on the gradual transformation of a sinusoidal beat-signal into well-separated pulses in a nonlinear and dispersive medium, the pulse repetition rate being simply determined by the frequency separation between the two continuous-wave (CW) laser sources. This all-optical technique has been successfully demonstrated with various experimental setups including dispersion-decreasing fibers [11], [12], adiabatic Raman compression in standard optical fibers [13] and step-like and comb-like dispersion profiled fibers [14]–[18]. However, these techniques often require a relatively complicated experimental setup and a careful management of the chromatic dispersion all along the fiber length.

More recently, this nonlinear compression effect has been observed through a multiple four-wave mixing (MFWM) process in a single anomalous dispersive optical fiber and has been proved to be an attractive and efficient technique to generate very high-repetition-rate pulse trains, combining both stability and simplicity of the experimental setup [19]–[23]. This powerful method has been successfully used for the generation of a 1.3-ps high-quality pulse train at 160 GHz [19], 11-ps pulses at 20 GHz [21], and subpicosecond pulses at 320 and 640 GHz [23].

In this work, we demonstrate the reliability of this technique for the generation of transform-limited Gaussian pulse trains at repetition rates ranging from 20 GHz up to 1 THz with a wavelength tunability over a 20-nm range. The first part of this paper presents an original theoretical description of the compression process. Numerical simulations based on the nonlinear Schrödinger equation (NLS) illustrate the pulse evolution from an initial beat-signal into a quasi-Gaussian pulse train. From these simulations, we also provide simple design rules that govern the optimum fiber length and the optimum input power as a function of fiber parameters. The second part is devoted to the experimental results. In a primary section, we describe for the first time the generation of a 40-GHz 4.7-ps pulse train through the MFWM process in a standard single mode fiber (SMF) as well as the generation of a 80-GHz 2.4-ps pulse train in a standard Teraligth fiber. Then, in order to provide an overview as large as possible of the possibilities of our method, we rapidly recall the results obtained at 20 and 160 GHz already published in [21] and [19], respectively. In the last sections of the paper, we describe the generation of 320- and 640-GHz

pulse trains at 1555 nm by means of a dispersion-flat highly nonlinear optical fiber (DF-HNLF). In particular, we complete the results published in [23] by making a comparison between two kinds of compression fiber and show that the reduction of third order dispersion is a crucial point to generate high quality subpicosecond pulses from 320-GHz and above. Furthermore, frequency resolved optical gating (FROG) analyses show that the phase of the 640-GHz pulses remains remarkably quite constant as a function of power, indicating that our sources can generate transform-limited pulses with a tunable width simply by adjusting the input average power. Finally, we experimentally demonstrate, for the first time of our knowledge, the generation of a 1-THz 170-fs well-separated pulse train at 1555 nm in a 90-m-long DF-HNLF.

II. Theoretical Approach

We consider linearly polarized light propagating in a single-mode optical fiber. Under the usual slowly varying field envelope approximation, the evolution of the electric field $u(z,t)$ is described by the following generalized NLS [24]:

$$\frac{\partial u}{\partial z} = -\frac{\alpha_l}{2}u - \frac{i}{2}\beta_2\frac{\partial^2 u}{\partial t^2} + \frac{1}{6}\beta_3\frac{\partial^3 u}{\partial t^3} + i\gamma\left(1+\frac{i}{\omega_0}\frac{\partial}{\partial t}\right)\left((1-fr)|u|^2 + fr\int_0^\infty R(t')|u(z,t-t')|^2dt'\right)u \quad (1)$$

where β_2 and β_3 are the second- and third-order dispersion coefficients, respectively, γ is the usual nonlinear coefficient, and α_l the linear fiber losses. fr represents the fractional contribution of the delayed Raman response to the nonlinear polarization. In the experiments described below, we found that fiber losses, Raman effect, and self-steepening do not affect significantly light propagation and can therefore be neglected. In fact, the main limiting effect is the third-order dispersion and note that high-quality pulses can be only obtained if $L\beta_3 \gg L\beta_2$, where $L\beta_3 = To^3/|\beta_3|^3$ and $L\beta_2 = To^2/|\beta_2|^2, To$ being the initial pulsewidth [24]. Under these assumptions, the propagation equation reduces to the usual NLS

$$\frac{\partial u}{\partial z} = -\frac{i}{2}\beta_2\frac{\partial^2 u}{\partial t^2} + i\gamma|u|^2u. \quad (2)$$

Let us consider now an initial beat-signal injected at the fiber input

$$u(0,t) = \sqrt{P_0/2}[\exp(-i\Omega t/2) + \exp(+i\Omega t/2)] \quad (3)$$

where P_0 is the initial average power and $\Omega/2\pi$ is the frequency separation between the two CW laser sources. A full-analytical approach of the propagation of a nonlinear beat-signal in an optical fiber has been performed by Trillo *et al.* in [20]. Based on a four modes model, their work shows that the dual-frequency pump mode, i.e., the initial sinusoidal signal, does not constitute a fixed point of the NLS equation and that additional sidebands will inevitably grow during the propagation in the optical fiber. The generation of these sidebands through a FWM process relies on the properties of the third-order susceptibility of the fiber medium: two pump photons at ω_1 and ω_2 interact to generate two first-order sideband photons located at $\omega_1 - \Omega$ and $\omega_2 + \Omega$, respectively, Ω being the pump frequency detuning: $\Omega = \omega_2 - \omega_1$. High-order sidebands are then generated due to MFWM. The efficiency of this FWM process and thus the number of generated sidebands depends on two parameters: the frequency separation between the pump waves Ω and the ratio between nonlinear and dispersion effects. More precisely, significant FWM occurs only if a phase-matching condition is satisfied [24]. In particular, the matching of the wave vectors depends on a relation between the group-velocity dispersion (GVD) and the nonlinear effects through the powers of the different waves involved in the compression mechanism [24]. In the strong pump depletion regime considered here, finding an analytical expression for the FWM phase-matching condition has proved to be a complex task, essentially because the powers of pumps and sidebands continuously evolve during the propagation. However, some physical insight can be obtained by numerically integrating (1). Fig. 1(a) represents the maximum of the first sideband intensity which can be obtained from the

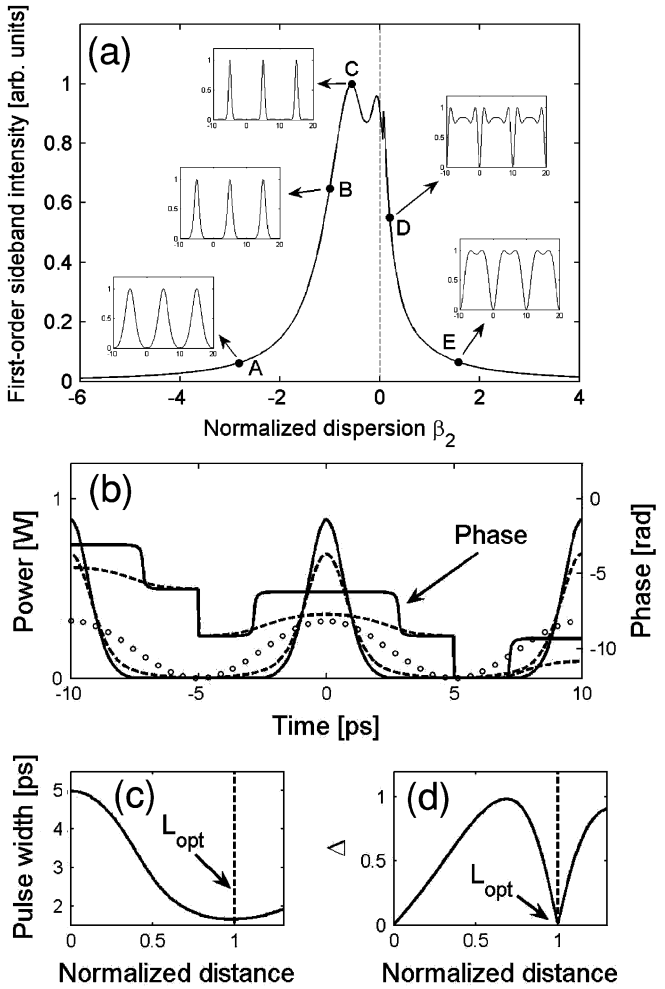

Fig. 1. (a) Evolution of the maximum of the first sideband intensity as a function of the normalized GVD. (b) Intensity and phase profiles at the fiber input $z = 0$ (circles) at the optimum fiber length $L_{\rm opt}$ (solid line) and at the distance corresponding to the maximum of Δ (dashed line). (c) Pulsewidth as a function of distance. (d) Evolution of the phase flatness as a function of distance.

FWM process as a function of the normalized GVD of the fiber and for a constant input power. From this curve, one can see that the FWM process only occurs over a limited range of GVD (phase-matching quasi-satisfied) and that sidebands can be generated both in anomalous and normal dispersion regimes. Nevertheless, note that the maximum gain is always located in the anomalous dispersion regime. Finally, the most interesting point is that in the anomalous dispersion regime, the spectral broadening leads to a significant compression of the initial beat-signal [points A, B, C in Fig. 1(a)], whereas in the normal dispersion regime, multiple FWM induces temporal broadening and formation of quasi-rectangular pulses [points D and E in Fig. 1(a)]. Recently, we have shown that for a suitable set of parameters, the initial beat-signal can evolve into a well-separated Gaussian pulse train during its propagation through the optical fiber [point B in Fig. 1(a)] [19]. This feature is illustrated in Fig. 1(b) which represents the signal intensity profiles at the fiber input (circles, $z = 0$) and at the fiber output (solid line, $z = 1$, distance normalized with respect to the optimum fiber length $L_{\rm opt}$ where maximum compression occurs) for the following normalized parameters: $\gamma = 1$ and $\beta_2 = -1$.

For the same set of parameters, we plot in Fig. 1(c) the evolution of the pulsewidth as a function of propagation distance. We can clearly see that there exists an optimum fiber length $z = 1$ which corresponds to the maximum compression ratio, i.e., minimum pulsewidth. An another important parameter that characterizes the pulse quality is the phase flatness which is calculated here using the following quantity:

$$\Delta = \frac{1}{T}\int \left|\frac{\partial \varphi}{\partial t}\right| dt.$$

With this definition, $\Delta = 0$ corresponds to chirp-free pulses (i.e., strictly flat phase over the entire pulsewidth). Fig. 1(d) shows the variation of Δ with the propagation distance. As can be seen, minimum Δ occurs also at the optimum distance $z = 1$ where the shortest transform-limited pulses are generated. This property is illustrated in Fig. 1(b) which shows the signal intensity (solid line) and its corresponding flat phase profile at the optimum fiber length output $(z = 1)$. Moreover, and quite remarkably, at a propagation distance corresponding to the maximum of $\Delta(z = 0.69)$ we found that the phase profile [dashed line in Fig. 1(b)] remains almost constant along the pulsewidth, indicating that phase variations are small with respect to the compression parameters and therefore that our source can generate quasi-transform-limited pulses with a tunable width, simply by adjusting the fiber length or the input average power.

Concerning the evolution of the pulse shape, more physical insight can be provided by noting that, during the nonlinear compression stage, the light intensity profile inside a period can be very well described by the superposition of a cosine function and a Gaussian function. That means that, at any distance z, the signal intensity can be approximated by the following fit function:

$$\begin{aligned} I_{\rm fit}(t,z) &= |u(z,t)|^2 \\ &= I_0(z) + k_1(z)\cos(\Omega t) + k_2(z)\exp(-k_3(z)t^2) \end{aligned} \tag{4}$$

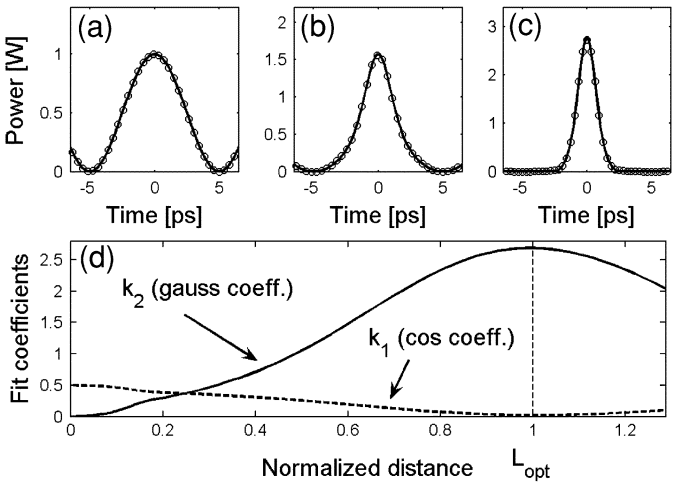

Fig. 2. (a) Initial beat-signal $(z = 0, k_1 = 0.5, k_2 = 0)$. (b) Pulse shape at $z = 0.5 (k_1 = 0.26, k_2 = 1.05)$. (c) Output signal at the optimum fiber length $(z = 1, k_1 = 0.02, k_2 = 2.7)$. In (a)–(c), circles represent the least squares fit of (4) to the pulse shape. (d) Evolution of the fit coefficients k_1 and k_2 as a function of the distance, normalized by the optimum fiber length $L_{\rm opt}$.

where $I_0(z)$ represents a continuous contribution. Moreover, by assuming that the whole energy is conserved during the propagation, we find the following relation between the fit coefficients:

$$I_0(z) = P_0 - \frac{k_2(z)\Omega}{2\sqrt{\pi k_3(z)}}. \tag{5}$$

The cosine amplitude $k_1(z)$ and the Gaussian amplitude $k_2(z)$ are simply obtained from a least squares fit of $I_{\rm fit}$ to the exact intensity profile calculated through numerical integration of (2). Fig. 2(a)–(c) illustrates the signal intensity profiles obtained from numerical integration (solid line) and the corresponding fit function (circles) at $z = 0, z = 0.5$, and $z = 1$, respectively. In addition, we plotted in Fig. 2(d) the evolution of the fit coefficients as a function of propagation distance during the pulse-formation process. As can be seen in this figure, the input beat-signal $(k_2 = 0)$ evolves very well towards a quasi-Gaussian pulse train $(k_1 \approx 0)$ at the optimum fiber output $(z = 1)$. We would like to emphasize that this remarkable property has been observed in the experiments described below.

Finally, all the results presented above emphasize the peculiar role played by the specific distance $L_{\rm opt}$. From a practical point of view, it would be interesting to derive expressions giving the optimum fiber length and average power in order to directly design a given pulse source. In this aim, we find from numerical simulations empirical relations binding the optimal fiber length $L_{\rm opt}$, the dispersion length $L_{\rm disp}$ and the nonlinear length $L_{\rm NL}$

$$L_{\rm opt} = a \times L_{\rm disp} = b \times L_{\rm NL}, \quad \text{with } a = 0.286; b = 2.571$$

and

$$L_{\rm disp} = \frac{1/(2f)^2}{|\beta_2|},\ L_{\rm NL} = \frac{1}{2\gamma P_{\rm opt}}. \tag{6}$$

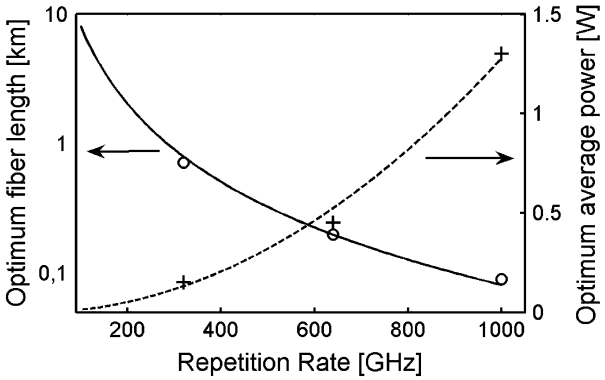

Fig. 3. Optimum fiber length and corresponding average input power as a function of repetition rate. Crosses and circles represent the experimental results of the 320-GHz, 640-GHz, and 1-THz pulse sources, respectively.

Then, from these relations, we obtain analytical expressions giving the optimal fiber length $L_{\rm opt}$ and average input power $P_{\rm opt}$ as a function of the repetition rate of the source and the fiber parameters

$$L_{\rm opt} = \frac{4\pi^2}{14|\beta_2|\Omega^2} \qquad P_{\rm opt} = \frac{16|\beta_2|\Omega^2}{4\gamma\pi^2}. \tag{7}$$

Fig. 3 illustrates how, in expressions (7), the optimum fiber length (solid line) and the optimum average power (dashed line) depend on the pulse train repetition rate for the following parameters: $\gamma = 0.011\ \mathrm{m}^{-1}\cdot\mathrm{W}^{-1}$ and $\beta_2 = -8.795 \times 10^{-4}\ \mathrm{ps}^2/\mathrm{m}$. Crosses and circles in Fig. 3 represent the optimum average power and fiber length experimentally obtained for 320 GHz, 640 GHz, and 1 THz, respectively. Clearly, an excellent agreement is observed between theoretical and experimental results, demonstrating the reliability of the empirical expressions (7) of $L_{\rm opt}$ and $P_{\rm opt}$ and thus allowing an easy, fast and reliable design of pulse sources.

In summary, we have theoretically shown in this first part that high-quality transform-limited Gaussian pulses can be obtained from a dual-frequency CW laser propagating in an anomalous dispersive fiber. Knowing both the fiber dispersion and nonlinearity, one can immediately rule the optimum fiber length and optimum average power using expressions (7).

III. Experimental Results

A. Experimental Setup

Fig. 4 represents the general experimental setup used to generate all the gigahertz/terahertz pulse trains. An initial beat-signal is synthesized through two continuous waves delivered by two tunable external-cavity lasers (ECLs) (ECL 1 and ECL 2) and combined by a 50:50 coupler. Repetition rate of the pulse source is simply determined by the frequency-separation between the two continuous waves. The generated beat-signal is then amplified to the optimum average power by means of an erbium-doped fiber amplifier (EDFA). The central wavelength of the laser diodes was first fixed to 1555 nm but can be shifted in the entire EDFA bandwidth. Because of the short linewidth of the ECLs (150 kHz), we would like to stress that one of the

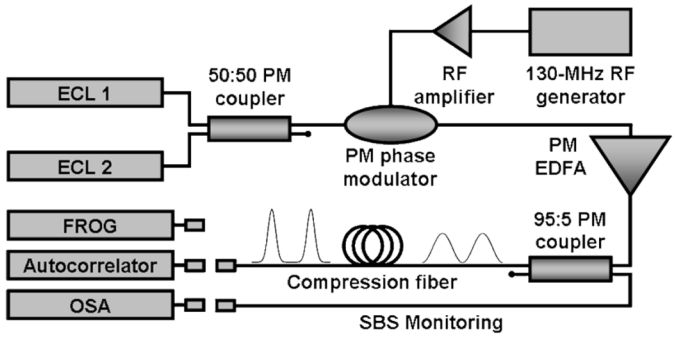

Fig. 4. Experimental setup.

key points of the injection setup is the use of a $LiNbO_3$ phase modulator driven at a frequency of 130 MHz which permits to dramatically increase the stimulated Brillouin scattering (SBS) threshold in the compression fiber (a few milliwatts in the 20-GHz 8-km-long SMF without phase modulator) well above the experimental average power and thus maximizing the MFWM process. Moreover, a 95:5 coupler was also placed at the compression fiber input to directly check the backward SBS signal during the whole experimental stage by means of an optical spectrum analyzer (OSA).

The second key point of the experimental setup is that the injection step is all made of polarization-maintaining (PM) fibers in order to maximize the FWM process in the compression fiber. Afterwards, the beat-signal is injected into the suitable optical fiber which is precisely chosen for each pulse source. Table I sums up the different features of fibers used for each source. The dispersion parameters were obtained using a chromatic-dispersion/optical time domain reflectometer (OTDR) device and were found to be in good agreements with those given by the manufacturer. The nonlinear coefficients of the SMF, TeraLight, and DF-HNLF were obtained from the effective area given by the manufacturer whereas the nonlinear coefficient of the nonzero dispersion shifted fiber (NZDSF) was measured using a modulated-instability (MI)-based measurement method [25].

After nonlinear reshaping in the optical fiber, the output field is finally characterized by means of an OSA, a background-free second-harmonic generation (SHG) autocorrelator and a FROG setup based on the OSA spectral analysis of the SHG autocorrelation signal [26]. The FROG trace is conveniently built up by adjusting the autocorrelator to a particular delay, and then scanning the OSA wavelength. The measured temporally-modulated spectra is finally interpolated onto a 512×512 grid, and used as input to the vector-based principal components generalized projections (PCGP) algorithm for the retrieval of the periodic pulse-train characteristics [26].

B. 40-GHz Results

Fig. 5 represents the experimental results obtained for the 40-GHz pulse source. The compression fiber is a 2.1-km-long SMF and the optimum average power was measured at 380 mW. Fig. 5(a) shows the measured and retrieved SHG-FROG traces of the field at the output of the SMF fiber. The FROG trace

TABLE I
FIBER PARAMETERS USED IN OUR EXPERIMENTS AT 1550 NM. (SMF: SINGLE MODE FIBER; NZDSF: NONZERO DISPERSION SHIFTED FIBER; DF-HNLF: DISPERSION FLAT HIGHLY NONLINEAR FIBER; D: CHROMATIC DISPERSION; S: DISPERSION SLOPE; γ: NONLINEAR COEFFICIENT; α: FIBER LOSSES; AND L: FIBER LENGTH.)

Repetition rate	Fiber Type	D (ps/km/nm)	S (ps/km/nm^2)	γ (W^{-1}km^{-1})	α (dB/km)	L (m)
20 GHz	SMF	17	0.055	1.3	0.22	7900
40 GHz	SMF	17	0.055	1.3	0.22	2100
80 GHz	Teraligth	6.2	0.06	1.7	0.2	1420
160 GHz	NZDSF	1	0.07	1.7	0.2	1000
320 GHz	NZDSF	0.38	0.07	1.7	0.22	1300
320 GHz	DF-HNLF	0.69	0.007	10.5	0.72	720
640 GHz	DF-HNLF	0.69	0.007	10.5	0.72	200
1 THz	DF-HNLF	0.69	0.007	10.5	0.72	90

exhibits a complex structure because of the generation of multiple FWM sidebands associated with the reshaping of the injected beat-signal. The retrieval error, defined as the root-mean-square (rms) between the original and retrieved FROG traces, was found to be $G = 5.9{\cdot}10^{-4}$. The corresponding retrieved intensity and phase are shown in Fig. 5(b). The retrieved intensity profile (solid line) shows well-separated reshaped pulses with clearly no pedestal. The phase variation over the compressed pulses is also negligibly small, indicating that pulses are essentially transform-limited. Results of the numerical simulations based on the generalized NLS equation including the parameters given by expressions (7) are also plotted in circles. We observe an excellent agreement between experimental (solid line) and numerical (circles) results indicating an easy and reliable design of our source. We can notice a π-jump phase between two consecutive pulses which originates from the initial beat-signal and which is conserved during the whole compression step in good agreement with numerical results of Fig. 1(a). Fig. 5(c) represents the least squares fit of a Gaussian function to the retrieved pulse shape. As can be clearly seen in this figure, the intensity profile corresponds very well to a Gaussian function, as predicted by the theoretical approach, with a 4.7-ps full-width at half-maximum (FWHM) which leads to a duty cycle of 5:1. The extinction ratio between peak power and interpulse background is better than 25 dB which stresses the high quality of the pulse source. Thanks to the method described in [27], we also experimentally evaluated the timing jitter of the source to $\sim$80 fs. Note that, for industrial applications, the timing jitter that originates from fluctuations of frequency difference between the two CW sources could be reduced by stabilizing the two ECLs through a single reference cavity, such as a Fabry–Perot resonator with a very high finesse [28]. Fig. 5(d) and (e) shows that the autocorrelation and spectrum derived from the retrieved pulse train (circles) are in excellent agreement with the independent direct experimental measurements (solid lines), thus confirming the reliability of the experimental setup and of the PCGP retrieval algorithm. Finally, the degree of tunability of the 40-GHz pulse source has been evaluated by studying the variation of the intensity FWHM (deconvoluted from the experimental autocorrelation trace) as a function of the central wavelength of the initial beat-signal. Fig. 5(f) shows that a tunability of more than 20 nm is achieved around 1555 nm. The insets in Fig. 5(f) show the experimental autocorrelation functions at 1543 and 1567 nm, respectively. Let us note that the main limitation of the wavelength tunability comes essentially from the fact that the two pumps have to be in the spectral bandwidth of our EDFA.

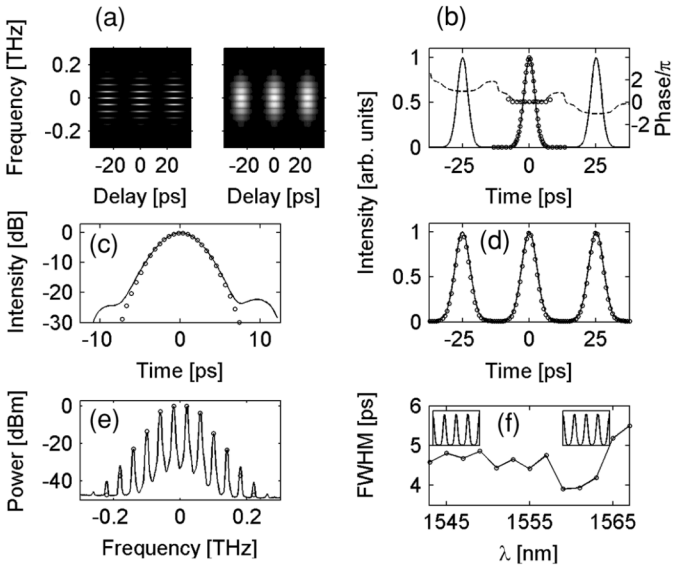

Fig. 5. (a) Measured (right) and retrieved (left) SHG-FROG traces of the generated 40-GHz pulse train. (b) Solid line shows the FROG retrieved intensity (left-hand axis), whereas dashed line shows the retrieved phase (right-hand axis), circles represent numerical simulation results. (c) Least squares fit of the retrieved pulse shape (solid line) by a Gaussian function (circles). (d) Measured autocorrelation function and (e) spectrum of the 40-GHz pulse train at the fiber output (solid curves). Circles represent the autocorrelation and spectrum calculated from the retrieved intensity and phase. (f) FWHM as a function of wavelength, insets show the experimental autocorrelation functions at 1543 and 1567 nm, respectively.

C. 20-GHz Results

Fig. 6 represents the experimental results obtained at 20 GHz for a SMF length of 7900 m. These results present the same features as those of Fig. 5. The FROG retrieval error is $8{\times}10^{-3}$. The retrieved intensity profile [Fig. 6(a), solid line] shows very well separated pulses obtained for an input average power of 130 mW, in excellent agreement with numerical simulations

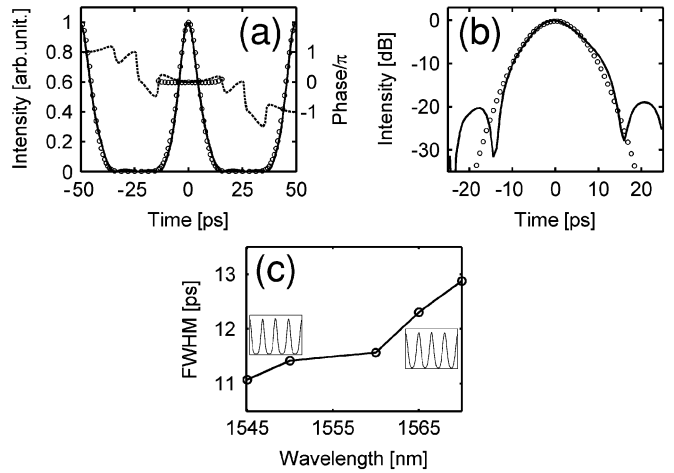

Fig. 6. (a) Retrieved intensity (solid line) and phase (dashed line) of the 20-GHz pulse train, numerical simulation results (circles). (b) Least squares fit of the retrieved pulse shape (solid line) by a Gaussian function (circles). (c) FWHM as a function of wavelength, insets show the experimental autocorrelation functions at 1545 and 1570 nm, respectively.

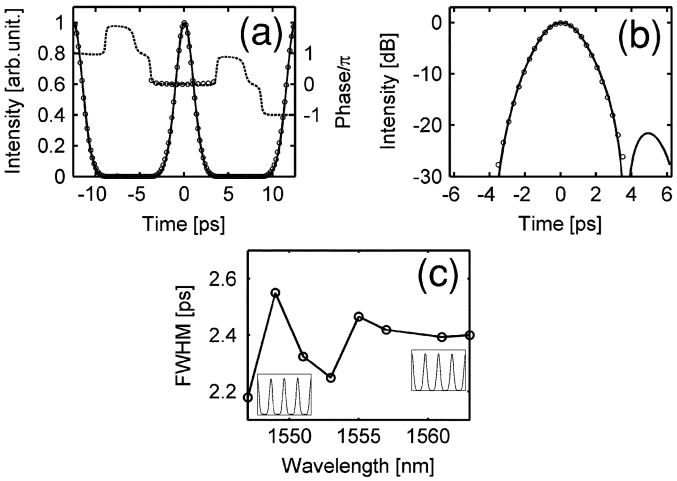

Fig. 7. (a) Retrieved intensity (solid line) and phase (dashed line) of the 80-GHz pulse train, numerical simulation results (circles). (b) Least squares fit of the retrieved pulse shape (solid line) by a Gaussian function (circles). (c) FWHM as a function of wavelength, insets show the experimental autocorrelation functions at 1547 and 1563 nm, respectively.

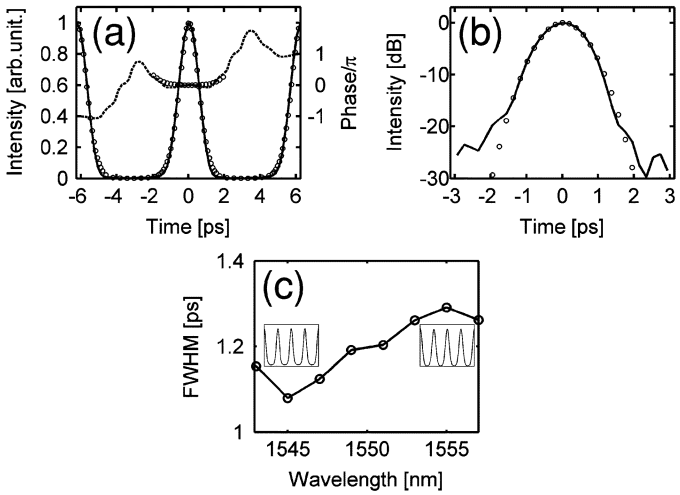

Fig. 8. (a) Retrieved intensity (solid line) and phase (dashed line) of the 160-GHz pulse train, numerical simulation results (circles). (b) Least squares fit of the retrieved pulse shape (solid line) by a Gaussian function (circles). (c) FWHM as a function of wavelength, insets show the experimental autocorrelation functions at 1540 and 1560 nm, respectively.

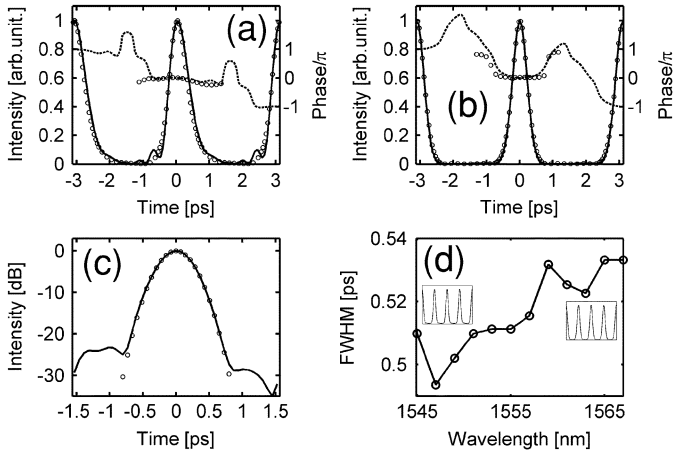

Fig. 9. (a) Retrieved intensity (solid line) and phase (dashed line) of the 320-GHz pulse train at the output of the 0.38 ps/km/nm NZDSF, numerical simulation results (circles). (b) Same as (a) but at the output of the 0.69 ps/km/nm DF-HNLF. (c) Least squares fit of the DF-HNLF retrieved pulse shape (solid line) by a Gaussian function (circles). (d) FWHM as a function of wavelength, insets show the experimental autocorrelation functions at 1545 and 1567 nm, respectively.

(circles). As in Fig. 5(b), the retrieved phase (dashed line) displays a π-jump between neighboring pulses and is almost constant over the compressed pulses, indicating that they are nearly transform-limited. The least squares fit of a Gaussian function to the retrieved pulse shape Fig. 6(b) corresponds very well to a Gaussian function with 11-ps FWHM, a duty cycle of 5:1 and an extinction ratio close to 20 dB [21]. Finally, Fig. 6(c) stresses that a wavelength tunability close to 20 nm is achieved around 1555 nm.

D. 80-GHz Results

Fig. 7 illustrates the results obtained at 80 GHz. The compression fiber was a standard Teraligth fiber whose parameters at 1550 nm are indicated in Table I. Fig. 7(a) (solid line) shows the retrieved intensity ($G = 2.4 \times 10^{-3}$) obtained for a fiber length of 1420 m and an input average power of 500 mW and corresponds nearly to transform-limited separated pulses. Results of numerical simulations (circles) are also plotted in Fig. 7(a). The least squares fit Fig. 7(b) is close to a Gaussian function with a 2.4-ps FWHM (duty cycle of 5:1) and an extinction ratio close to 20 dB; note that pulses are accompanied by a -20-dB satellite pulse. Finally, a 15-nm wavelength tunability was observed around 1555 nm [Fig. 7(c)].

E. 160-GHz Results

As shown in the theoretical section, increasing the repetition rate of the pulse sources requires lower dispersions and higher powers. In this context, the 160-GHz pulse compression setup was basically made of a NZDSF whose parameters at 1550 nm

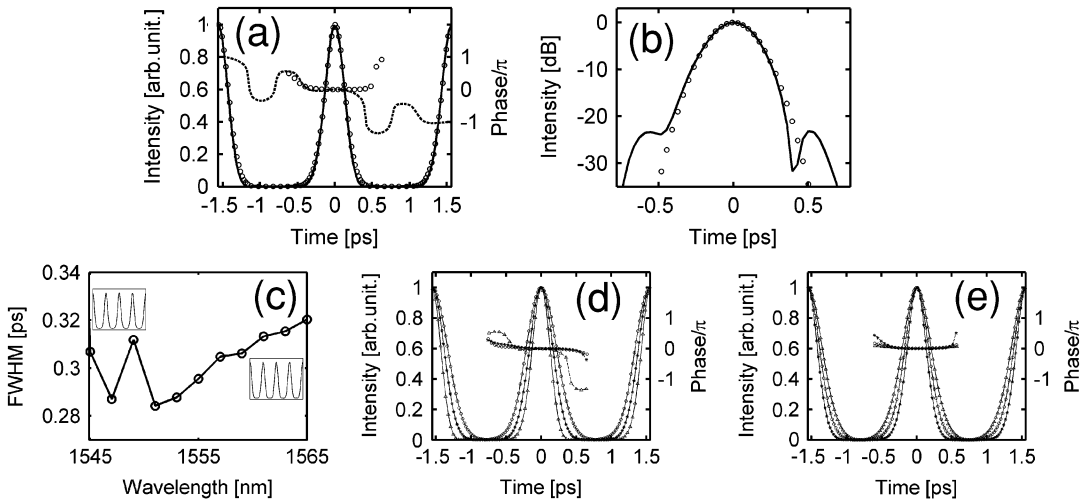

Fig. 10. (a) Retrieved intensity (solid line) and phase (dashed line) of the 640-GHz pulse train, numerical simulation results (circles). (b) Least squares fit of the retrieved pulse shape (solid line) by a Gaussian function (circles). (c) FWHM as a function of wavelength, insets show the experimental autocorrelation functions at 1545 and 1565 nm, respectively. (d) Retrieved intensity (solid line) and phase (dashed line) of the 640-GHz pulse train as a function of input average power, 450 mW (triangles), 340 mW (crosses), and 240 mW (circles). (e) Numerical simulation results corresponding to (d).

are summed up in Table I. Fig. 8 represents the 160-GHz experimental results obtained for a NZDSF length of 1 km and an input average power of 525 mW. Fig. 8(a) (solid line) shows the FROG retrieved intensity profile ($G = 3 \times 10^{-3}$). It corresponds pretty well to transform-limited separated pulses with remarkably no pedestal. The least squares fit [Fig. 8(b)] is close to a Gaussian function with 1.27-ps FWHM (duty cycle of 5:1) and an extinction ratio better than 20 dB [19]. Results of numerical simulations (circles) are also plotted in Fig. 8(a) and prove again that excellent predictions had been done. Finally, the wavelength tunability of the 160-GHz pulse source was measured close to 20 nm around 1550 nm [Fig. 8(c)].

F. 320-GHz Results

As repetition rate increases, high order effects, such as third-order chromatic dispersion (TOD), become non negligible and dramatically limit the compression factor and quality of output pulses. Indeed, to obtain pulse sources with FWHM less than 1 ps, fibers with low dispersion slope are required in order to satisfy $L\beta_3 \gg L\beta_2$ [23]. So as to illustrate this point, we have carried out two series of experiments. The first 320-GHz pulse source was designed thanks to a 1300-m NZDSF whose parameters at 1550 nm are given in Table I. The maximum compression factor experimentally occurs for an input average power of 380 mW. The FROG results are presented in Fig. 9(a) (FROG retrieval error i5.4s $\times 10^{-3}$). We can see that the retrieved intensity profile [Fig. 9(a), solid line] shows separated pulses with a FWHM of 670 fs but presents small pedestals and mainly a large asymmetry due to TOD. Note that numerical simulation results (circles) are in good agreement with the experiment and have correctly predicted the present pulse asymmetry. To overcome this pulse asymmetry, we substituted the NZDSF for a DF-HNLF from OFS whose parameters are specified in Table I. Fig. 9(b)–(d) represent the experimental results obtained at 320 GHz for a DF-HNLF length of 720 m. The FROG retrieval error was found to be $G = 3.3 \times 10^{-3}$. The intensity profile (solid line) shows very well-separated pulses with no more asymmetry and remarkably no pedestal for this ultrahigh repetition rate. Maximum compression is obtained for an input average power of 150 mW leading to a FWHM of only 500 fs (duty cycle of 6:1), in excellent agreement with numerical simulations (circles). The retrieved phase (dashed line) is almost constant over the compressed pulses, indicating that pulses are nearly transform-limited. The least squares fit [Fig. 9(c)] is close to a Gaussian function with a good symmetry and an excellent extinction ratio close to 25 dB. Finally, the degree of tunability of the 320-GHz pulse source has been evaluated to be more than 20 nm around 1555 nm.

G. 640-GHz Results

Fig. 10 represents the experimental results obtained at 640 GHz for a DF-HNLF length of 200 m. These results present the same features as those obtained at 320-GHz (Fig. 9). The FROG retrieval error is relatively small, $G = 2.4 \times 10^{-3}$. The retrieved intensity profile [Fig. 10(a), solid line] shows very well-separated pulses, nearly transform-limited, with a FWHM of 300 fs obtained for an input average power of 450 mW, in excellent agreement with numerical simulations (circles). The least squares fit [Fig. 10(b)] is close to a Gaussian function with an excellent extinction ratio better than 20 dB. Moreover, Fig. 10(c) stresses a wavelength tunability of more than 20 nm around 1555 nm. Finally, we carried out three different FROG measurements as a function of the input DF-HNLF average power. Fig. 10(d) shows the FROG results for an input power of 450 mW (triangles), 340 mW (crosses), and 240 mW (circles). We can clearly see that pulses become narrower as the average power increases until P_{opt} where the maximum Gaussian compression ratio is reached. Remarkably, the phase of pulses remains quite constant as a function of power, in good agreement with numerical results of Fig. 10(e) and theoretical approach of Fig. 1(a), indicating that the optimum average power is not critical for the pulse chirp. In other words, our sources can generate transform-limited pulses with a tunable width by simply adjusting the input average power.

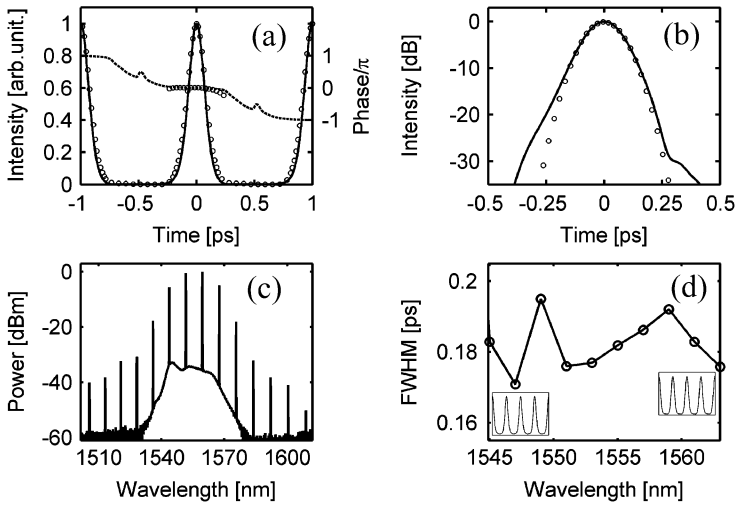

Fig. 11. (a) Retrieved intensity (solid line) and phase (dashed line) of the 1-THz pulse train, numerical simulation results (circles). (b) Least squares fit of the retrieved pulse shape (solid line) by a Gaussian function (circles). (c) Measured spectrum of the generated 1-THz pulse train. (d) FWHM as a function of wavelength, insets show the experimental autocorrelation functions at 1545 and 1563 nm, respectively.

H. 1-THz Results

Fig. 11 represents the final experimental results obtained at the ultrahigh repetition rate of 1 THz for a DF-HNLF length of 90 m. The FROG retrieval error was found to be relatively small, $G = 1.9\times10^{-3}$. The retrieved intensity profile [Fig. 11(a), solid line] shows well-separated, high-quality, nearly transform-limited pulses with a FWHM of only 170 fs obtained for an input average power of 1.3 W. Results of numerical simulations (circles) are also plotted in Fig. 11(a) and prove again that good numerical predictions have been done by means of expressions (7). The least-squares fit Fig. 11(b) is close to a Gaussian function with an excellent extinction ratio close to 25 dB and the peak power of the pulses after nonlinear reshaping in the optical fiber was nearly equal to 7 W. The measured spectrum is also plotted in Fig. 11(c); note the multiple generated FWM sidebands associated with the beat-signal compression and the poor number of sidebands contains in the EDFA bandwidth which forbid any further EDFA amplification. On the other hand, this is the only limit of our method as well; indeed, the two initial pumps have to be in the amplification bandwidth of our EDFA, which limits the maximum repetition rate up to $\sim$3 THz. Finally, Fig. 11(d) stresses that a wavelength tunability of more than 20 nm is achieved around 1555 nm.

IV. Conclusion

In summary, we have studied numerically and experimentally the generation of pico- and femtosecond pulse trains at very high repetition rates using a highly efficient nonlinear compression technique. This method is based on the gradual transformation of a sinusoidal beat-signal into Gaussian pulses through a MFWM process taking place in an anomalous dispersive optical fiber. The reliability of this simple and powerful technique was demonstrated for the generation of high-quality transform-limited Gaussian pulses at 20, 40, 80, 160, 320, 640 GHz, and 1 THz over a 20-nm wavelength range around 1555 nm. The FROG technique was used to accurately characterize the intensity and phase of the generated pulse trains and retrieved results were found to be in very good agreements with those obtained from numerical integration of the NLS equation. Moreover, we provide simple design rules to obtain both the optimum fiber length and the optimum input average power as a function of the repetition rate of the source and fiber parameters. Finally, we believe that this compression technique, tunable in wavelength, pulsewidth and repetition rate, could find a large number of applications in many areas of ultrafast physics including ultrahigh-capacity optical communication systems, clock generation, and optical waveform measurement.

References

[1] H. G. Weber, S. Ferber, M. Kroh, C. Schmidt-Langhorst, R. Ludwig, V. Marembert, C. Boerner, F. Futami, S. Watanabe, and C. Schubert, "Single channel 1.28 Tbit/s and 2.56 Tbit/s DQPSK transmission," presented at the ECOC 2005 Glasgow, U.K., Post-Deadline Paper Th4.1.2.

[2] M. Nakazawa, Y. Yamamoto, and K. R. Tamura, "1.28 Tbit/s-70 km OTDM transmission using third- and fourth-order simultaneous dispersion compensation with a phase modulator," *Electron. Lett.*, vol. 36, pp. 2027–2029, 2000.

[3] G. Meloni, G. Berrettini, M. Scaffardi, A. Bogoni, L. Poti, and M. Guglielmucci, "250-times repetition frequency multiplication for 2.5-THz clock signal generation," *Electron. Lett.*, vol. 41, pp. 1294–1295, 2005.

[4] H. Takara, S. Kawanishi, and M. Saruwatari, "Optical signal eye diagram measurement with subpicosecond resolution using optical sampling," *Electron. Lett.*, vol. 32, pp. 1399–1400, 1996.

[5] A. Hirata, M. Harada, and T. Nagatsuma, "120-GHz wireless link using photonic techniques for generation, modulation and emission of millimeter-wave signals," *J. Lightw. Technol.*, vol. 21, no. 5, pp. 2145–2153, Sep.-Oct. 2003.

[6] T. Yamamoto, E. Yoshida, and M. Nakazawa, "Ultrafast nonlinear optical loop mirror for demultiplexing 640 Gbit/s TDM signal," *Electron. Lett.*, vol. 34, pp. 1013–1014, 1998.

[7] A. Bogoni, M. Scaffardi, P. Ghelfi, and L. Poti, "Nonlinear optical loop mirrors: Investigation solution and experimental validation for undesirable counterpropagating effects in all-optical signal processing," *IEEE J. Sel. Topics Quantum Electron.*, vol. 10, no. 10, pp. 1115–1123, Oct. 2004.

[8] D. Massoubre, J. L. Oudar, J. Fatome, S. Pitois, G. Millot, J. Decobert, and J. Landreau, "All-optical extinction ration enhancement of a 160 GHz pulse train using a saturable absorber vertical microcavity," *Opt. Lett.*, vol. 31, pp. 537–539, 2006.

[9] A. Hasegawa, "Generation of a train of soliton pulses by induced modulational instability in optical fibers," *Opt. Lett.*, vol. 9, pp. 288–290, 1984.

[10] K. Tai, A. Hasegawa, and A. Tomita, "Observation of modulation instability in optical fibers," *Phys. Rev. Lett.*, vol. 56, pp. 135–138, 1986.
[11] P. V. Mamyshev, S. V. Chernikov, and E. M. Dianov, "Generation of fundamental soliton trains for high-bit-rate optical communication lines," *IEEE J. Quantum Electron.*, vol. 27, no. 10, pp. 2347–2355, Oct. 1991.
[12] S. V. Chernikov, E. M. Dianov, D. J. Richardson, R. I. Laming, and D. N. Payne, "114 Gbit/s soliton train generation through Raman self-scattering of a dual frequency beat signal in dispersion decreasing optical fiber," *Appl. Phy. Lett.*, vol. 63, pp. 293–295, 1993.
[13] A. D'errico, C. Loiacono, M. Presi, G. Contestabile, and E. Ciaramella, "Widely tunable 40 GHz pulse source for 160 Gbit/s OTDM by simultaneous soliton generation and compression," presented at the ECOC 2003, Rimini, Italy, Paper We 2.6.5.
[14] Y. Ozeki, S. Takasaka, T. Inoue, K. Igarashi, J. Hiroishi, R. Sugizaki, M. Sakano, and S. Namiki, "Nearly exact optical beat-to-soliton train conversion based on comb-like profiled fiber emulating a polynomial dispersion decreasing profile," *IEEE Photon. Technol. Lett.*, vol. 17, no. 8, pp. 1698–1700, Aug. 2005.
[15] S. V. Chernikov, J. R. Taylor, and R. Kashyap, "Comblike dispersion-profiled fiber for soliton pulse train generation," *Opt. Lett.*, vol. 19, pp. 539–541, 1994.
[16] M. Tadakuma, O. Aso, and S. Namiki, "A 104 GHz 328 fs soliton pulse train generation through a comb-like dispersion profiled fiber using short high nonlinearity dispersion shifted fiber," presented at the OFC 2000, Baltimore, MD, Paper ThL3.
[17] S. V. Chernikov, J. R. Taylor, and R. Kashyap, "Experimental demonstration of step-like dispersion profiling in optical fibre for soliton pulse generation and compression," *Electron. Lett.*, vol. 30, pp. 433–435, 1994.
[18] S. V. Chernikov, R. Kashyap, M. J. Guy, D. G. Moodie, and J. R. Taylor, "Ultrahigh-bit-rate optical sources and applications," *Phil. Trans. Roy. Soc. Lond. A*, vol. 354, pp. 719–731, 1996.
[19] S. Pitois, J. Fatome, and G. Millot, "Generation of a 160 GHz transform-limited pedestal-free pulse train through multiwave mixing compression of a dual-frequency beat signal," *Opt. Lett.*, vol. 27, pp. 1729–1731, 2002.
[20] S. Trillo, S. Wabnitz, and T. A. B. Kennedy, "Non linear dynamics of dual-frequency-pumped multiwave mixing in optical fibers," *Phys. Rev. A.*, vol. 50, pp. 1732–1747, 1994.
[21] S. Pitois, C. Finot, J. Fatome, B. Sinardet, and G. Millot, "Generation of 20-GHz picosecond pulse trains in the normal and anomalous dispersion regimes of optical fibers," *Opt. Commun.*, vol. 260, pp. 301–306, 2006.
[22] J. F. L. Freitas, C. J. S. de Matos, and A. S. L. Gomes, "Simultaneous pulse train generation and wavelength conversion in a highly nonlinear fibre due to multiwave mixing," presented at the ECOC 2005, Glasgow, U.K., Paper Mo 4.5.5.
[23] J. Fatome, S. Pitois, and G. Millot, "320/640 GHz high-quality pulse sources based on multiple four-wave mixing in highly nonlinear optical fibre," *Electron. Lett.*, vol. 41, pp. 1391–1392, 2005.
[24] G. P. Agrawal, *Nonlinear Fiber Optics*. New York: Academic, 2001.
[25] J. Fatome, S. Pitois, and G. Millot, "Measurement of nonlinear and chromatic dispersion parameters of optical fibers using modulation instability," *Opt. Fiber Technol.* , vol. 12, no. 3, pp. 243–250, Jul. 2006.
[26] R. Trebino, K. W. Delong, D. N. Fittinghoff, J. N. Sweetser, M. A. Krumbugel, B. A. Richman, and D. J. Kane, "Measuring ultrashort laser pulses in the time-frequency domain using frequency-resolved optical gating," *Rev. Sci. Instrum.*, vol. 68, pp. 3277–3295, 1997.
[27] J. Dörring, G. B. Tudury, A. Lenihan, G. M. Carter, and Y. J. Chen, "All optical timing jitter measurements on 40 Gbit/s pseudorandom RZ data after long-haul transmission in dispersion-managed soliton system," *Electron. Lett.*, vol. 38, pp. 727–729, 2002.
[28] A. Schoof, J. Grünert, S. Ritter, and A. Hemmerich, "Reducing the linewidth of a diode laser below 30 Hz by stabilization to a reference cavity with a finesse above 10^5," *Opt. Lett.*, vol. 26, pp. 1562–1564, 2001.

Julien Fatome was born in Charleville-Méziéres, France in 1978. After graduating from ESIREM, Dijon, France, he received the DEA degree in 2000 and the Ph.D. degree in physics for studies of ultra-short pulse propagation at 160-Gb/s in dispersion managed optical fiber lines in 2004, both from the University of Bourgogne, Dijon, France.

In 2005, he became a Research Engineer in the Centre National de la Recherche Scientifique (CNRS), Department of Physics, University of Bourgogne. He is currently carrying out research in nonlinear effects and pulse trains propagation at ultrahigh bit rate in optical fibers.

Stéphane Pitois was born in Beaune, France, in 1974. He received the Ph.D. degree in physics for studies of modulational instability and domain walls in optical fibers from the University of Burgundy, Dijon, France, in 2000.

He then carried out postdoctoral research with the Department of Optics and Acoustics, Free University of Brussels, Brussels, Belgium, on nonlinear effects in dynamical Bragg gratings. In 2001, he became a Researcher at the Centre National de la Recherche Scientifique (CNRS), Department of Physics, University of Burgundy. He has published over 70 contributions in journals, books, and conference proceedings. His research interests include nonlinear effects and pulse trains propagation in optical fibers.

Guy Millot was born in Alligny-en-Morvan, France, in 1960. He received the Ph.D. degree in laser Raman spectroscopy in gases from the University of Burgundy, Dijon, France, in 1986.

Since 1994, he is a Full Professor with the Physics Department, University of Burgundy. His research interests have been focused on nonlinear effects in optical fibers, modulational instabilities, solitons, generation, propagation and characterization of optical pulse trains at high repetition rates, stimulated Raman scattering, frequency conversion, and applications in optical communications. He has published over 150 contributions in journals, books, and conference proceedings.

Dr. Millot is a member of the Institut Universitaire de France (IUF) since 2000. In 2004, he received the Silver Medal from the CNRS.